NeuroResource

Neuron

A New DREADD Facilitates the Multiplexed Chemogenetic Interrogation of Behavior

Highlights

- Structure-guided approach for κ-opioid receptor (KOR)-DREADD (KORD) design
- KORD is selectively activated by salvinorin B, and not by endogenous opioids
- KORD robustly silenced multiple neuronal subtypes
- Inhibitory KORD combined with excitatory hM3Dq for multiplexed behavioral control

Authors

Eyal Vardy, J. Elliott Robinson, ..., Michael J. Krashes, Bryan L. Roth

Correspondence

michael.krashes@nih.gov (M.J.K.), bryan_roth@med.unc.edu (B.L.R.)

In Brief

The κ-opioid receptor (KOR) was used as a template to generate a novel inhibitory DREADD (KORD), which is activated by salvinorin B and insensitive to endogenous opioid peptides. Sequential activation of the inhibitory KOR-DREADD and an excitatory M3-DREADD facilitated the bidirectional, multiplexed modulation of behavior.

Vardy et al., 2015, Neuron *86*, 936–946
May 20, 2015
http://dx.doi.org/10.1016/j.neuron.2015.03.065

CellPress

CellPress

Neuron
NeuroResource

A New DREADD Facilitates the Multiplexed Chemogenetic Interrogation of Behavior

Eyal Vardy,[1,8] J. Elliott Robinson,[2,3,4,8] Chia Li,[5,6,8] Reid H.J. Olsen,[1,3] Jeffrey F. DiBerto,[2] Patrick M. Giguere,[1] Flori M. Sassano,[1] Xi-Ping Huang,[1] Hu Zhu,[1] Daniel J. Urban,[1] Kate L. White,[1] Joseph E. Rittiner,[3] Nicole A. Crowley,[1,3,4] Kristen E. Pleil,[1,3,4] Christopher M. Mazzone,[1,3,4] Philip D. Mosier,[7] Juan Song,[1,3] Thomas L. Kash,[1,3,4] C.J. Malanga,[2,3,4] Michael J. Krashes,[5,6,*] and Bryan L. Roth[1,3,*]

[1]Department of Pharmacology and National Institute of Mental Health Psychoactive Drug Screening Program (NIMH PDSP)
[2]Neurology Department
University of North Carolina School of Medicine, Chapel Hill, NC 27514, USA
[3]Curriculum in Neurobiology
[4]Bowles Center for Alcohol Studies
University of North Carolina School of Medicine, Chapel Hill, NC 27599, USA
[5]Diabetes, Endocrinology, and Obesity Branch, National Institute of Diabetes and Digestive and Kidney Diseases, National Institutes of Health, Bethesda, MD 20892, USA
[6]National Institute of Drug Abuse, Baltimore, MD 21224, USA
[7]Department of Medicinal Chemistry, Virginia Commonwealth University School of Pharmacy, Richmond, VA 23298, USA
[8]Co-first author
*Correspondence: michael.krashes@nih.gov (M.J.K.), bryan_roth@med.unc.edu (B.L.R.)
http://dx.doi.org/10.1016/j.neuron.2015.03.065

SUMMARY

DREADDs are chemogenetic tools widely used to remotely control cellular signaling, neuronal activity, and behavior. Here we used a structure-based approach to develop a new G_i-coupled DREADD using the kappa-opioid receptor as a template (KORD) that is activated by the pharmacologically inert ligand salvinorin B (SALB). Activation of virally expressed KORD in several neuronal contexts robustly attenuated neuronal activity and modified behaviors. Additionally, co-expression of the KORD and the G_q-coupled M_3-DREADD within the same neuronal population facilitated the sequential and bidirectional remote control of behavior. The availability of DREADDs activated by different ligands provides enhanced opportunities for investigating diverse physiological systems using multiplexed chemogenetic actuators.

INTRODUCTION

Over the past several years, optogenetic and chemogenetic (Armbruster et al., 2007; Boyden et al., 2005) approaches have transformed neuroscience and other disciplines by facilitating the reversible, cell type-specific control of cellular signaling and electrical activity. As complementary technologies, opto- and chemogenetics have demonstrated robust utility for deconstructing the neuronal codes responsible for both simple and complex behaviors (Deisseroth, 2011; Sternson and Roth, 2014). The chemogenetic platform known as DREADDs (designer receptors exclusively activated by designer drugs) has proven to be extremely useful for interrogating cellular signaling in cell types as diverse as glia (Agulhon et al., 2013), pancreatic β-cells (Guettier et al., 2009; Jain et al., 2013), hepatocytes (Li et al., 2013), triple-negative breast cancer cells (Yagi et al., 2011), transformed fibroblasts (Vaqué et al., 2013), and induced pluripotent stem (iPS) cells (Dell'Anno et al., 2014).

Current DREADDs, activated by the inert clozapine metabolite clozapine-N-oxide (CNO), can silence (Armbruster et al., 2007) or enhance (Alexander et al., 2009) neuronal firing, and can modulate cellular signaling via G_i, G_q, G_s, or β-arrestin cascades (Guettier et al., 2009; Nakajima and Wess, 2012). However, the dependence of DREADD technology on the same inert ligand CNO limits its effectiveness for bidirectional and multiplexed chemogenetic control of neuronal and non-neuronal activity. Thus, the development of a new DREADD that can be activated by a distinct chemotype would represent a powerful new tool for neuroscientists and biologists in general.

The first chemogenetic tool based on a G protein-coupled receptor (GPCR) was developed by Strader and colleagues in 1991 (Strader et al., 1991). Since then, many orthologous receptor-ligand pairs have been developed (e.g., RASSLs, TRECs, neoceptors, and so on; Conklin et al., 2008), though with occasionally limited utility. Common problems associated with these first-generation chemogenetic tools included the following:

(1) Many of the synthetic compounds that activate the modified receptors exhibit appreciable affinities and potencies for the native receptors. This nonselective activity limits their efficacy in vivo because of the need to employ knockout animals in order to avoid activation of endogenous receptors.
(2) In some cases, ligand potency was too low to be useful for studies in vivo.
(3) The selectivity profile of the ligands was typically unspecified (e.g., they may have activities at other unidentified cellular targets).

(4) Many of the previously reported modified receptors had high basal signaling in vivo that obscures ligand-induced phenotypes (Rogan and Roth, 2011).

The recent development of engineered ligand-gated ion channels (PSAMs and PSEMs) overcomes many of these deficiencies (Magnus et al., 2011), although because PSAMs and PSEMs are ion channels, they have limited value in non-excitable cells.

Here we reveal the development of a new DREADD using the κ-opioid receptor (KOR) as a template that is activated by salvinorin B (SALB). Since SALB is an inactive, drug-like metabolite of the KOR-selective agonist salvinorin A (SALA) (Ansonoff et al., 2006; Roth et al., 2002), and because SALB has excellent CNS penetrability and pharmacokinetic properties in both rodents and non-human primates (Hooker et al., 2009), the SALB/KORD combination will be exceptionally suited for a variety of contexts. Additionally, the SALB/KORD pairing facilitates the multiplexed chemogenetic interrogation of GPCR signaling and behavior.

RESULTS

SALB Is Inert In Vivo

Previous preliminary studies showed that SALB is pharmacologically inert in vitro and in vivo (Ansonoff et al., 2006). To verify and extend these findings, we profiled SALB against a large number of CNS molecular targets using the resources of the National Institute of Mental Health Psychoactive Drug Screening Program as described in Besnard et al. (2012) and Keiser et al. (2009). SALB failed to show any activity except the previously reported low KOR [^{3}H]-diprenorphine radioligand binding affinity (K_i = 2.95 μM; Figure 1H). Importantly, SALB was also inactive at muscarinic receptor-based DREADDs (G_q, G_i, and G_s DREADDs; Figure S1). We found that SALB is a weak KOR agonist with an EC_{50} of 248 nM (Figure 1D; Table 1). Importantly, the potency of SALB is so weak that even after i.c.v. administration SALB failed to produce KOR-mediated anti-nociception, while SALA (its active precursor) was potently analgesic (Ansonoff et al., 2006).

Given both the weak potency of SALB at wild-type (WT) KOR and its inactivity when administered i.c.v., we reasoned that SALB will be inactive in vivo. To test this hypothesis, we used several behavioral assays to determine whether SALB can induce behavioral effects commonly associated with KOR agonists: analgesia, impairment of motor performance, and the production of anhedonic-like states. First, we measured the analgesic and ataxic effects of SALB and compared its activity with a metabolically stable SALA analog, MOM-ether SALB (MOM-B), using hot plate and rotarod assays, respectively. While 2.0 mg/kg MOM-B produced effects in both the hot plate and rotarod tests, administration of 10.0 mg/kg SALB did not alter performance relative to controls (Figures 1A and 1B). Subsequently, we used the curve-shift method of intracranial self-stimulation (ICSS) to detect reward-devaluing effects of SALB. While SALA (0.1–1.0 mg/kg) significantly elevated brain stimulation reward thresholds in C57BL/6J mice at all doses tested ($F_{3,\ 18}$ = 14.5, $p < 0.001$; Figures 1C and S4), SALB (3.0–17.0 mg/kg) failed to significantly elevate thresholds up to 17.0 mg/kg s.c. Given that SALB is apparently inert in vivo, and because of its outstanding pharmacokinetic and CNS penetrability properties (Hooker et al., 2009), we predicted that SALB would represent a suitable ligand for a new DREADD.

Structure-Based Design of KORD

In order to develop a new DREADD, we initially hoped to evolve the human KOR (hKOR) to be responsive to SALB using our yeast-based directed molecular evolution approach (Armbruster et al., 2007; Dong et al., 2010). For these studies, hKOR was cloned into the yeast expression plasmid p416 and functionally expressed in a genetically modified strain of *S. cerevisiae*, which enables ligand-induced activation of heterologously expressed mammalian G_i-coupled GPCRs to engage the pheromone-signaling pathway, thereby promoting growth on selective media (Dong et al., 2010; Erlenbach et al., 2001; Noble et al., 2003). We created a library of mutant hKOR receptors by random mutagenesis, and screened them for activation by SALB. We were able to identify multiple mutants activated by SALB, although they all displayed high levels of constitutive activity, rendering them relatively useless for the studies we envisioned.

Therefore, we employed a rational approach to designing the KOR DREADD based on our recent crystallographic, mutagenesis, and molecular modeling studies of hKOR (Vardy et al., 2013; Wu et al., 2012). These studies showed that an alanine mutation at E297 at the extracellular end of TM6 (an important residue in KOR specificity determinant, in the so-called ''address domain''; Larson et al., 2000) causes a 10-fold decrease in the affinity and potency of the endogenous peptide ligand dynorphin A (DYNA) without altering the affinity or potency of SALA (Vardy et al., 2013). Another residue, D138 in TM3, which belongs to the general opioid activation determinant, was also examined. This residue resides in the ''message domain'' of KOR (Portoghese, 1989; Vardy et al., 2013), and D138A mutations have been reported to nearly abolish the binding of all known KOR agonists without affecting the affinity or potency of SALA (Kane et al., 2006; Vardy et al., 2013). Furthermore, recent high-resolution crystal structures of related opioid receptors (Fenalti et al., 2014, 2015) implied that this residue is also essential for the interaction of other classes of opioids including opioid peptides and opioid antagonists. We reasoned, therefore, that changing the negative charge to a polar residue via a D138N mutation would further decrease the potency of endogenous peptide ligands and enhance the potency of SALB and SALA.

Indeed, the D138N mutation apparently abolished DYNA (1–13) agonist efficacy and potency and diminished peptide binding affinity while enhancing SALA and SALB affinities and potencies 10- to 30-fold (see Figures 1D and 1F–1H; Table 1). As a key requisite of DREADDs is the failure to be activated by endogenous neurotransmitters, we combined these two KOR mutants (e.g., D138N/E297A) and evaluated the resulting construct. Both the double D138N/E297A mutant and the single D138N mutant responded to SALB and SALA with greatly enhanced potencies compared to WT, while the E297A mutant alone had no effect on SALB agonist potency (Figure 1D). Critically, the single D138N mutant was not activated by any tested synthetic or endogenous peptide KOR ligands (Figure 1G; Table 1). Thus, in a screen of 21 endogenous opioids performed

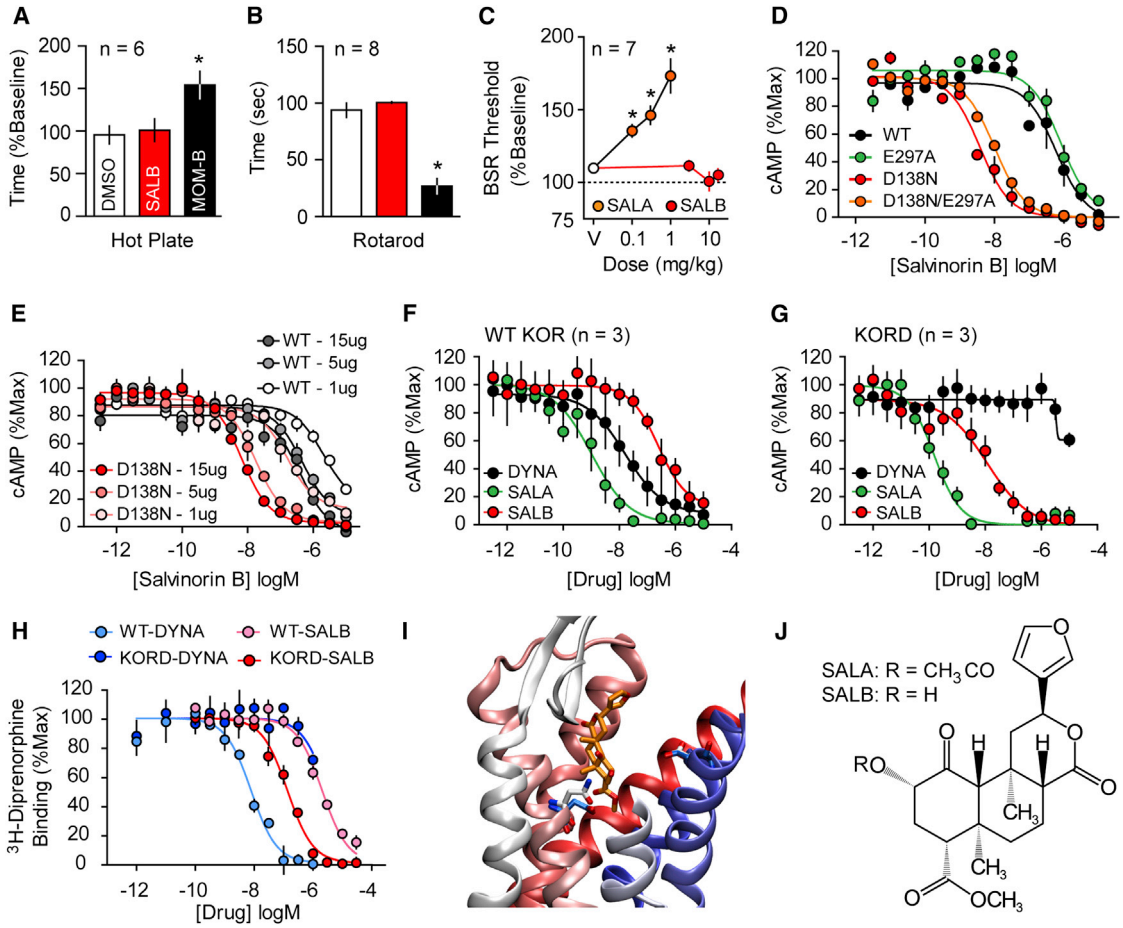

Figure 1. Rational Design and In Vitro Characterization of KORD

(A and B) SALB was initially validated as a DREADD ligand by demonstrating its apparent pharmacologic inertness in vivo using behavioral tests by comparing with MOM-SALB via (A) hot plate test and (B) impairment of motor performance using the rotarod test. In both tests SALB effects (red) were compared to vehicle (white) and a stabilized variant of SALA (MOM-SALB, black).

(C) The lack of production of a KOR-like anhedonic state was tested using ICSS and compared to the effects of SALA. Data represent mean ± SEM of indicated number of separate experiments.

(D) We characterized the KORD comparing the G_i-mediated response of different KOR mutants and demonstrate an increased potency of SALB at D138N-containing mutants.

(E) The effect of receptor expression levels on SALB potency of WT KOR (gray) and KORD (red). As can be seen, DNA concentration is directly related in both WT-KOR and KORD to agonist potency yielding a right shift in potency of 1–2 orders of magnitude.

(F and G) Average G_i response of WT-KOR (F) and KORD (G) to classic KOR ligands dynorphin A (DYNA, black), SALA (green), and the inert compound SALB (red) is shown.

(H–J) (H) Competition binding isotherms of WT and KORD for DYNA (1–13) (pK_i values, 8.50 ± 0.12 and 5.79 ± 0.06, respectively) and SALB (pK_i values, 5.53 ± 0.08 and 6.98 ± 0.13, respectively). An examination of a model of KORD docked with SALB (I) suggests that the DREADD mutation (D138N) eliminates unfavorable interactions between D138 and SALB. In WT KOR, D138 is turned away from the ligand-binding site (cyan), while N138 in KORD (white) is interacting directly with the ligand. E297 in both models assumes the same conformation reflecting the fact that it has no effect on DREADD activity. Deacetylation at position 2 of SALA results in SALB (J). Asterisk indicates $p < 0.05$, and all values reported as mean ± S.E.M.

at WT and the D138N mutants, no opioid peptide was found to have detectible agonist activity at the D138N mutant (Table 1; Figure 1G). As the D138N mutant is potently activated by the inactive drug SALB and apparently not activated by any tested endogenous peptide agonist, we chose it as our candidate DREADD and have dubbed it KORD (κ-opioid DREADD).

GPCR overexpression typically results in a large degree of receptor reserve thereby enhancing agonist potency. Thus, because a high level of receptor reserve can be easily achieved for DREADDs via virally mediated transduction, receptor reserve could further enhance the apparent affinity, selectivity, and potency of SALB for the KORD. To test this notion, we transfected HEK293T cells with increasing concentrations of plasmids expressing either WT hKOR or the KORD (D138N hKOR), which resulted in varying levels of receptor expression. As predicted, increased receptor expression levels correlated with an increase in the apparent potency of SALB (Figure 1E). Significantly, the potency differences between cells expressing levels

Table 1. KORD Is Insensitive to Endogenous Opioid Peptides and Is Potently Activated by SALB

	hKOR		KORD	
	EC_{50} (nM) pEC_{50} ± SEM	Emax (%)	EC_{50} (nM) pEC_{50} ± SEM	Emax (%)
β-Endorphin (1–27) (β-Endor1–27) YGGFMTSEKSQTPLVLFKNAIIKNAY	700 6.15 ± 0.22	100	NA	NA
β-Endorphin (1–31) (β-Endor1–31) YGGFMTSEKSQTPLVLFKNAIIKNAYKKGE	706 6.15 ± 0.17	100	NA	NA
Leu-enkephalin (Leu-Enk) YGGFL	NA	NA	NA	NA
Met-enkephalin (Met-Enk) YGGFM	2,099 5.68 ± 0.12	79	NA	NA
Met-enkephalin-Arg-Phe (MERF) YGGFMRF	1,344 5.87 ± 0.14	99	NA	NA
Metorphamide YGGFMRRV-NH2	108 6.99 ± 0.07	97	NA	NA
BAM 12 YGGFMRRVGRPE	101 6.99 ± 0.07	99	NA	NA
BAM 18 YGGFMRRVGRPEWWMDYQ	85 7.07 ± 0.09	97	NA	NA
BAM 22 YGGFMRRVGRPEWWMDYQRYG	93 7.03 ± 0.07	95	NA	NA
Peptide E YGGFMRRVGRPEWWMDYQRYGGFL	65 7.18 ± 0.07	95	NA	NA
Dynorphin A(1–6) (DynA1–6) YGGFLR	227 6.64 ± 0.24	86	NA	NA
Dynorphin A(1–7) (DynA1–7) YGGFLRR	107 6.97 ± 0.04	97	NA	NA
Dynorphin A(1–8) (DynA1–8) YGGFLRRI	122 6.91 ± 0.06	94	NA	NA
Dynorphin A(1–9) (DynA1–9) TGGFLRRIR	127 6.89 ± 0.07	93	NA	NA
Dynorphin A(1–13) (DynA1–13) YGGFLRRIRPKLK	19 7.71 ± 0.06	94	NA	NA
Dynorphin A(1–17) (DynA1–17) YGGFLRRIRPKLKWDNQ	13 7.87 ± 0.09	100	NA	NA
Dynorphin B(1–13) (DynB1–13) YGGFLRRQFKVVT	120 6.91 ± 0.08	100	NA	NA
Leumorphin YGGFLRRQFKVVTRSQEDPNAYYEELFDV	21 97.68 ± 0.06	92	NA	NA
α-Neoendrophin (α-neo-End) YGGFLRKYPK	64 7.19 ± 0.07	95	NA	NA
Endomorphin-1 YPWF	NA	NA	NA	NA
Endomorphin-2 YPFF	NA	NA	NA	NA
Nociceptin FGGFTGARKSARKLANQ	1,007 5.99 ± 0.07	81	NA	NA
U69593	3.16 8.5 ± 0.1	100	> 10,000	NA
Salvinorin B (low expression)	2,045 5.68 ± 0.18	80	160 6.79 ± 0.13	94
Salvinorin B (high expression)	248 6.6 ± 0.1	100	11.8 7.98 ± 0.09	100
Salvinorin A (low expression)	19.8 7.71 ± 0.08	100	0.12 9.91 ± 0.08	100
Salvinorin A (high expression)	1.05 8.96 ± 0.08	100	0.04 10.35 ± 0.08	100

NA, no activation at 10 μM. Data represent mean EC_{50} and mean pEC_{50} ± SEM of n = 3 separate 16-point dose-response experiments each performed in triplicate. hKOR, human κ-opioid receptor; KORD, κ-opioid receptor DREADD.

of WT receptor (achieved using 1 μg DNA), which is at a level similar to endogenous brain expression, versus cells expressing high levels of the mutant receptor (achieved using 15 μg DNA), is close to 1,000-fold (Figure 1E). Thus, our rationally designed KORD greatly enhances hKOR sensitivity to SALB and simultaneously abolishes the agonist activity of a variety of endogenous and exogenous KOR agonists (Figure 1G; Table 1).

As constitutive activity is a potential confounding issue with respect to overexpressed chemogenetic and optogenetic tools, we next examined the constitutive activity of KORD compared to both a WT and a constitutively active KOR mutant (V108L). We found that the basal activity of KORD (137 ± 3.7 × 10^5 lumens/min; n = 44; p > 0.05 versus WT) was equivalent to WT (134 ± 3.2 × 10^5 lumens/min; n = 48) and less than the V108L constitutively active mutant (94 ± 3.7 × 10^5 lumens/min; n = 50; p < 0.001 versus WT), indicating that the KORD does not represent an apparently constitutively active mutant. Although the atomic mechanisms responsible for the increased affinity and potency for SALB are unknown, our modeling results suggest that it is likely due to the removal of an unfavorable desolvation cost associated with non-basic ligand binding to a charged aspartate (Asp) (Vardy et al., 2013). Indeed, our docking studies suggest that changing the Asp at this position to asparagine (Asn) results in an improved conformation for the Asn, decreases the energetic cost for desolvation, and thus increases affinity (see Figure 1I).

In Vivo Neuronal Validation of KORD

KORD Activation Induces Neuronal Hyperpolarization

To test the activity of the KORD in vivo, we used a standard Cre-recombinase-dependent adeno-associated virus (AAV), which enabled the targeting of KORD to specific neuronal populations in different Cre-driver mouse lines (Figure 2A). We verified effective transduction of KORD in a Cre-dependent manner in a variety of neurons, including the substantia nigra (SN) and the ventral tegmental area (VTA) of vesicular GABA transporter (VGAT)-*ires*-Cre mice (Figures 2B and 2C), the paraventricular hypothalamus (PVH) of single-minded1 (SIM1)-Cre mice (Balthasar et al., 2005), and the arcuate nucleus (ARC) of agouti-related peptide (AGRP)-*ires*-Cre mice (Tong et al., 2008) (Figures 3A, 3B, 3E, and 3F).

We next performed whole-cell patch clamp recordings in acutely prepared slices to test the ability of KORD to generate a SALB-induced hyperpolarization. Results were calculated as a shift from baseline resting membrane potential (RMP). In VTA/SN-VGAT-expressing (VTA/SN^{VGAT}) neurons transduced with KORD, bath application of SALB led to a robust and significant membrane potential hyperpolarization, while SALB had no effect on control (mCherry-transduced) neurons (t_9 = 2.97, p < 0.05; Figure 2D). To determine the generalizability of KORD-mediated hyperpolarization, we also evaluated SIM1-expressing neurons in the PVH (PVH^{SIM1}) and AgRP-expressing neurons in the ARC (ARC^{AgRP}). Upon bath application of SALB, both PVH^{SIM1} and ARC^{AgRP} neurons expressing KORD exhibited robust hyperpolarization, shifting −6.2 ± 2.1 mV and −10.1 ± 1.7 mV, respectively (PVH^{SIM1}, t_5 = 2.99, p < 0.05; ARC^{AgRP}, t_4 = 5.94, p < 0.05; Figures 3D and 3H). Next, we sought to determine if the KORD can act presynaptically to inhibit neurotransmission by recording miniature inhibitory postsynaptic currents (mIPSCs) in VTA/SN neurons in the presence of SALB. In VGAT-*ires*-Cre mice with AAV-hSyn-DIO-KORD injected into the VTA/SN, SALB significantly reduced mIPSC frequency (t_2 = 24.7, p < 0.001; Figure 2E), but not amplitude (t_2 = 2.45, p > 0.05) compared to baseline, consistent with a presynaptic effect. SALB had no effect on mIPSCs in naive mice (frequency, t_2 = 0.92, p > 0.05; amplitude, t_2 = 4.1, p > 0.05). No differences in baseline mIPSC frequency were observed between AAV-hSyn-DIO-KORD-injected mice and naive mice (Figure 2E).

Peripheral SALB Administration Produces Robust Behavioral Responses

Given that SALB induced KORD-mediated hyperpolarization, we next tested whether the SALB-induced activation of KORD had functional consequences on three distinct neuronal populations: (1) VTA/SN^{VGAT}, (2) hypothalamic PVH^{SIM1}, and (3) hypothalamic ARC^{AgRP} (using VGAT-*ires*-Cre, SIM1-Cre, and AGRP-*ires*-Cre mice, respectively). Since previous studies have demonstrated that optogenetic modulation of VTA/SN^{VGAT} neurons can modify locomotion (van Zessen et al., 2012), we predicted that chemogenetic silencing via KORD of VTA/SN^{VGAT} neurons (Figures 2B and 2C) would increase locomotion. As expected, SALB produced a dose-dependent increase in locomotor activity ($F_{3, 21}$ = 19.1, p < 0.001) (Figure 2F), while vehicle was without effect; post hoc testing revealed that the 1.0-, 3.0-, and 10.0-mg/kg SALB doses significantly enhanced locomotion. Importantly, mice expressing mCherry in the same neuronal population were unresponsive to SALB (Figure 4B).

Next, we evaluated KORD activity in a neural circuit known to be involved in feeding behavior. PVH^{SIM1} neurons (Figures 3A and 3B), which make up the vast majority of PVH cells, have been previously demonstrated to increase food intake when chemogenetically inhibited (Atasoy et al., 2012; Stachniak et al., 2014). Consistent with prior results obtained using hM4Di, SALB activation of KORD in PVH^{SIM1} neurons significantly increased feeding behavior compared to baseline (0.61 ± 0.04 g versus 0.06 ± 0.01 g; t_6 = 11.8, p < 0.05; Figure 3C), whereas WT control mice (t_5 = 0.30, p < 0.05) injected with the Cre-dependent KORD virus had no feeding effects in response to the administration of SALB.

As a final test, we evaluated the orexigenic ARC^{AgRP} neurons (Figures 3E and 3F), which have been shown to send inhibitory projections to the PVH and synapse onto a subpopulation of PVH^{SIM1} neurons (Krashes et al., 2014; Atasoy et al., 2012). Having established that activation of KORD hyperpolarizes PVH^{SIM1} neurons in vitro and increases food intake in vivo, we next tested KORD activation with SALB on the upstream inhibitory ARC^{AgRP} neurons (Figures 3G and S2). Following light cycle food restriction, food consumption was monitored during the first 60 min of the dark cycle, when mice normally eat and ARC^{AgRP} neural activity is high (Krashes et al., 2011). Compared to vehicle (0.59 ± 0.07 g), KORD inhibition of the hunger-promoting ARC^{AgRP} neurons resulted in significantly diminished levels of food intake (0.11 ± 0.03 g; t_5 = 11.29, p < 0.05). Importantly, SALB administration did not impact feeding responses in WT animals (vehicle, 0.52 ± 0.05 g; SALB, 0.55 ± 0.07 g).

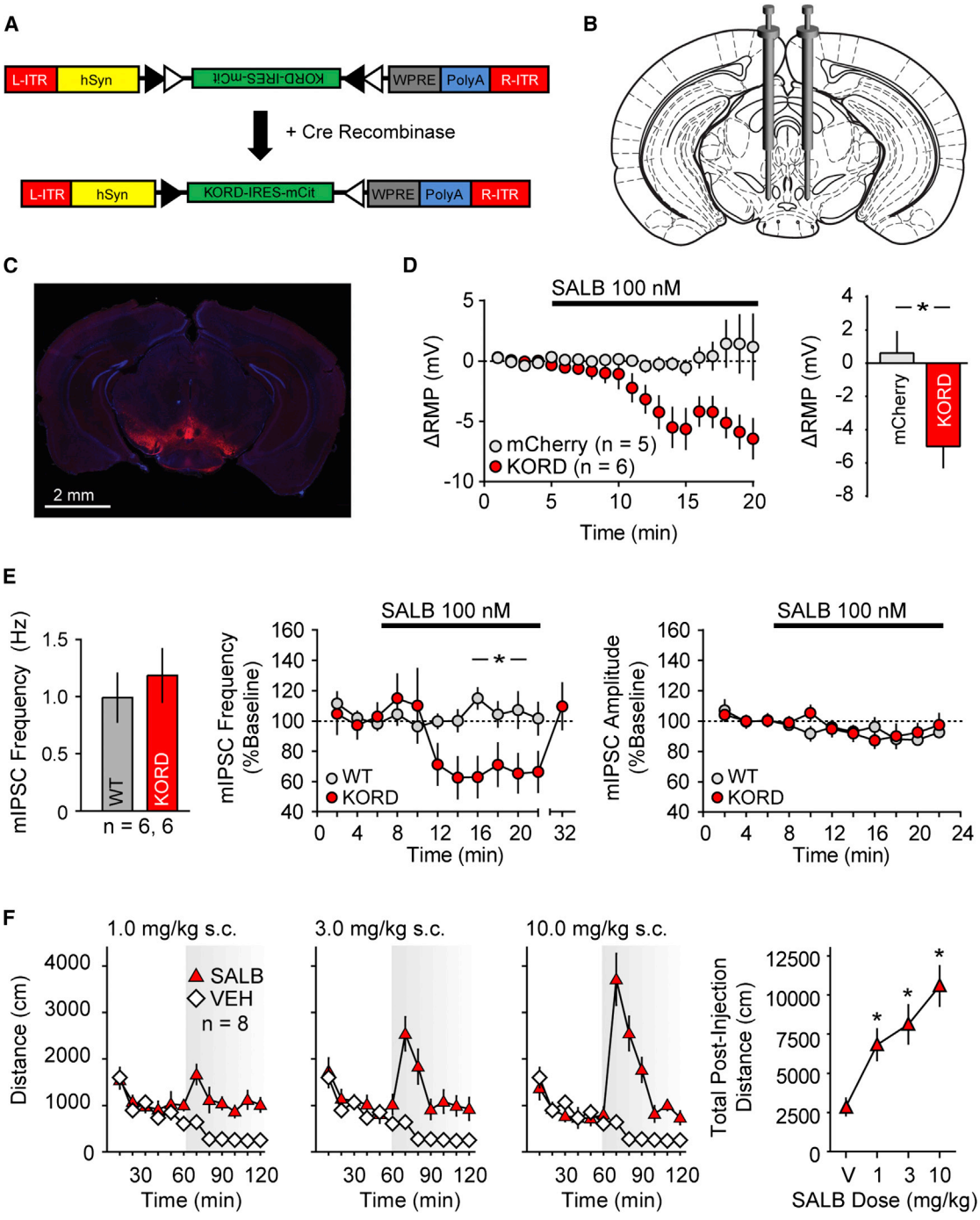

Figure 2. Validation of KORD In Vivo in VTA/SN^{VGAT} Neurons

(A) Schematic showing the AAV8 (hSyn-DIO-hKORD-IRES-mCit-WPRE-PolyA-R-ITR) construct used and its recombination under the control of Cre-recombinase.

(B) Location for viral infusion of Cre-expressing VTA/SN^{VGAT} neurons.

(C) Representative low-power field of VTA/SN^{VGAT} neurons.

(D) Shift from baseline resting membrane potential (RMP) in VTA/SN^{VGAT} neurons transduced with KORD or mCherry (control) constructs.

(E) Baseline mIPSC frequency in non-KORD-expressing neurons in KORD-infected mice and control neurons from naive mice controls and the effects of SALB on miniature IPSC frequency and amplitude in uninfected VTA/SN^{VGAT} and naive control VTA/SN neurons.

(F) Locomotor responses for graded doses of SALB. Asterisk indicates $p < 0.05$, and all values reported as mean ± S.E.M.

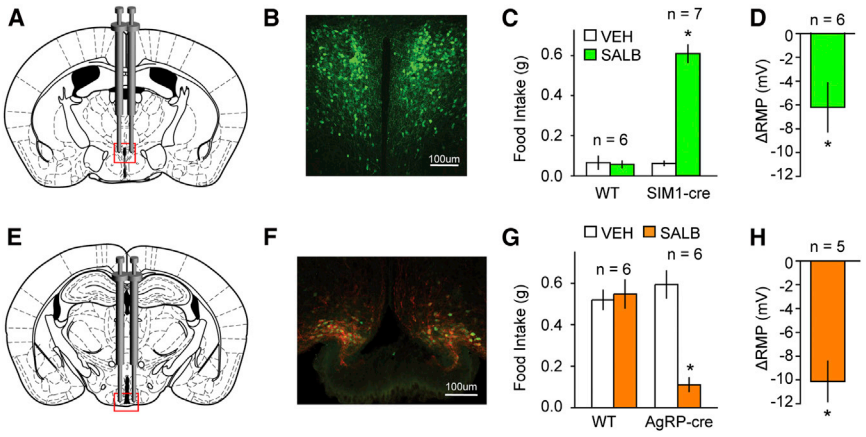

Figure 3. Validation of KORD In Vivo in PVH^{SIM1}- and ARC^{AgRP}-Expressing Neurons

(A) Location for viral infusion of PVH^{SIM1} Cre-expressing neurons.

(B) Representative immunofluorescent photomicrographs demonstrating expression of mCitrine in virally transduced neurons.

(C) Effects of SALB on food intake in AAV-hSyn-DIO-KORD-injected SIM1-Cre and WT mice.

(D) Shift from baseline resting membrane potential (RMP) in KORD-transduced neurons in the PVH^{SIM1}.

(E and F) Location of viral infusion and expression of mCitrine (green) and HA-hKORD (red) in ARC^{AgRP} neurons.

(G) Suppression of food intake by SALB.

(H) Shift from baseline RMP in KORD-transduced neurons in the ARC^{AgRP}. Asterisk indicates $p < 0.05$, and all values represent mean ± S.E.M.

KORD Facilitates Chemogenetic Multiplexed Control of Behavior

One of our main goals for developing the KORD was to enable multiplexing experiments for either the simultaneous or sequential manipulation of neuronal pathways using a variety of chemo- and optogenetic platforms. To test whether two distinct DREADDs can reciprocally modulate neuronal activity and behavior in vivo, we transduced VTA/SN^{VGAT} neurons or hypothalamic ARC^{AgRP} neurons with both the inhibitory, G_i-coupled, SALB-activated KORD and the stimulatory, G_q-coupled, CNO-activated hM3Dq. We then tested for receptor expression and behavioral effects.

We found that locomotor activity could be bidirectionally modulated by KORD and hM3Dq in the same mouse. During different testing sessions, SALB (10.0 mg/kg) enhanced locomotor activity in mice that expressed both KORD and hM3Dq in VTA/SN^{VGAT} neurons compared to vehicle ($t_4 = 2.89$, $p = 0.04$; Figure 4B), and CNO (3.0 mg/kg) decreased locomotor activity ($t_4 = 5.44$, $p = 0.006$). When tested during the same session, CNO (3.0 mg/kg) produced significant locomotor depression ($t_4 = 3.28$, $p = 0.03$), while SALB (17.0 mg/kg) rescued the effects of CNO and significantly elevated locomotor activity when compared to vehicle ($t_4 = 3.44$, $p = 0.03$; Figures 4C and 4D). In these sessions, the onset of action of both CNO and SALB began influencing locomotor behavior within 10–20 min post-injection. Importantly, neither SALB (10.0 mg/kg; $t_5 = 1.93$, $p > 0.05$) nor CNO (3.0 mg/kg; $t_5 = 0.95$, $p > 0.05$) had any effect on locomotor activity in control mice expressing mCherry in VTA/SN^{VGAT} neurons (Figure 4B). Histologic analysis of VTA/SN^{VGAT} neurons showed that 87.7% ± 1.7% of transduced neurons co-expressed both receptors with no significant difference in the transduction efficiency of either DREADD ($t_2 = 0.82$, $p > 0.05$; Figure S3). These results demonstrate for the first time that two different biologically inert designer ligands can produce robust behavioral changes in the same mouse, providing the first proof of concept for multiplexed chemogenetic control of behavior.

We next investigated the effectiveness of multiplex manipulation of behavior while transducing ARC^{AgRP} neurons with both the hM3Dq and KORD. As acute opto- and chemogenetic activation of ARC^{AgRP} neurons drives feeding behavior (Aponte et al., 2011; Betley et al., 2013; Krashes et al., 2011), we attempted to reverse ARC^{AgRP} hM3Dq activation-induced feeding with simultaneous KORD inhibition. Importantly, for this experiment to work, extensive restraint of ARC^{AgRP} neuron activity is necessary to overcome the chemogenetically induced feeding response, given that only ~10% of ARC^{AgRP} neurons are required to drive the full magnitude of food intake (Aponte et al., 2011; Betley et al., 2013). Consistent with previous studies, CNO/hM3Dq-induced activation of ARC^{AgRP} neurons increased light cycle food intake (0.75 ± 0.03 g) significantly compared to saline baseline (0.04 ± 0.02 g; Time, $F_{6,\ 108} = 108.4$; Treatment, $F_{1,\ 18} = 10.6$; and Time × Treatment, $F_{6,\ 108} = 4.5$; $F_{6,\ 108} = 62.1$, $p < 0.001$ for all; Figure 4E). However, co-administration of CNO and SALB significantly blunted feeding behavior (CNO versus CNO + SalB; Time, $F_{6,\ 108} = 80.9$; Treatment, $F_{1,\ 18} = 204.3$; and Time × Treatment, $F_{6,\ 108} = 62.1$; $p < 0.001$ for all). Post hoc testing revealed a significant reduction of food intake similar to that observed during simultaneous optogenetic activation and hM4Di-mediated inhibition of ARC^{AgRP} neurons (Stachniak et al., 2014). Interestingly, these animals elevate their feeding rate in the next 2 hr (1–3 hr after ligand injection), reflecting both the transient action of SALB/KORD and persistent action of CNO/hM3Dq (Figure 4E).

DISCUSSION

Here we report the development of a new chemogenetic tool based on the KOR we have dubbed KORD (κ-opioid DREADD). We demonstrate that KORD can be used alone or in conjunction with other chemogenetic tools, thereby facilitating the multiplexed dissection of neural circuitry and behavior. As KORD is activated by SALB, it can be used in mice also expressing CNO-responsive DREADDs, allowing for the first time bidirectional chemogenetic manipulation of neural circuits. Although bidirectional control has only been demonstrated in the hypothalamus and VTA/SN, it is likely that this approach will work in other brain regions. The KORD could also be used together with other chemogenetic and optogenetic tools in order to provide higher-order multiplexed modulation of GPCR signaling in non-neuronal cells.

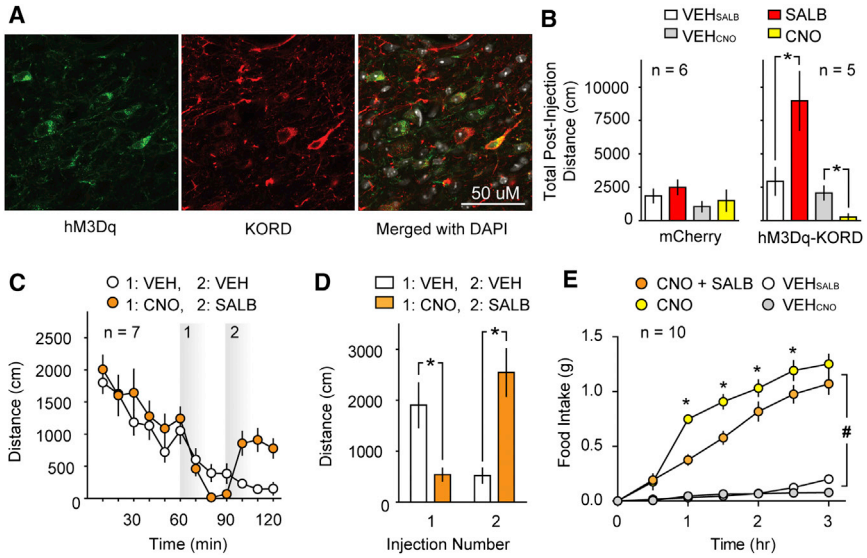

Figure 4. Multiplexed Bidirectional Chemogenetic Control of Behavior

(A) Representative immunofluorescent confocal micrographs wherein hM3Dq and KORD were co-expressed in VTA/SN^{VGAT} neurons with co-localization data summarized in Figure S3.

(B) Comparison of the effects of CNO and SALB on spontaneous locomotor activity of dual DREADD-expressing mice (right panel; mice expressing both hM3Dq and KORD in VTA/SN^{VGAT} neurons) or control mice (mCherry; left panel). CNO inhibits spontaneous locomotor behavior, and SALB augments locomotor behavior on different testing days (right panel). CNO and SALB did not affect behavior in mice that expressed mCherry in the same brain region.

(C) Bidirectional manipulation of locomotor behavior: the locomotor activity of dual DREADD-expressing mice was inhibited by CNO (CNO injection at 60 min). The locomotor depression was reversed by SALB injection (SALB injection 30 min after CNO injection).

(D) Summary data of locomotor activity experiments using multiplexed DREADDs.

(E) Demonstration that SALB inhibits food intake induced by CNO-mediated activation of hM3Dq when both are expressed in ARC^{AgRP} neurons; these effects show transient effects of SALB versus the persistent effects of CNO. Asterisk indicates $p < 0.05$, and all values represent mean ± S.E.M.

The kinetics of CNO on neuronal activation via hM3Dq have been demonstrated thoroughly by a large number of independent studies, with in vivo DREADD-mediated responses beginning 5–10 min after IP injection, and peak electrophysiological response occurring 45–50 min after injection (Alexander et al., 2009; Urban and Roth, 2015). It has also been reported by many labs that both the behavioral and electrophysiological effects of CNO-mediated DREADD activation can persist for several hours following a single injection in a manner predicted by its pharmacokinetic properties (Urban and Roth, 2015). By contrast, SALA and SALB concentrations in the rodent and primate brain increase within a few seconds following parenteral administration and then rapidly decline ($t_{1/2}$ = 10–15 min; Hooker et al., 2009). Likewise, the behavioral effects of SALB in KORD-expressing mice begin and peak shortly after injection, yielding a behavioral effect that lasts for approximately 1 hr with the doses administered here. As a prolonged activation of DREADDs by CNO may be a problem when studying rapidly modulated, short-term behaviors, the apparently brisk onset of the effects of SALB in KORD-expressing mice may prove valuable for such studies. Indeed, prior studies have demonstrated that SALB is cleared quickly from the brain, but has a slightly more prolonged plasma half-life (Hooker et al., 2009), and thus its pharmacokinetic properties may be better suited for studies in which relatively acute neuronal silencing is required, while CNO-based DREADDs (e.g., hM4Di) are useful where prolonged silencing is desired.

Given that SALB has some modest activity at KOR, it is possible that neurons with a high degree of receptor reserve could show responses to high systemically administered doses of SALB. Even though we have been unable to detect any pharmacological effect of SALB administration, it will be important to avoid using excessively high doses (e.g., > 10 mg/kg) and to test SALB in animals in which KORD has not been expressed. Additionally, because of the limited solubility of SALB, it will be important going forward to develop analogs of SALB which show improved water solubility.

Optogenetic and chemogenetic tools have revolutionized neuroscience research by facilitating the region- and cell type-specific manipulation of neuronal activity. Optogenetics provides inherent advantages with millisecond temporal resolution, although the hardware required for precise intracranial light delivery is not only invasive, but also cumbersome in comparison to the minimal requirements for chemogenetic manipulation. Chemogenetic control via DREADDs provides slower kinetics due to the systemic administration of CNO or SALB, but has demonstrated its ability to achieve the same functional mapping results with less invasive intervention (reviewed by Mahler et al., 2014; Stachniak et al., 2014; Urban and Roth, 2015). It is also possible to directly infuse CNO into specific brain structures to obtain a transient and focal DREADD activation. The newly developed KORD described here provides potentially greater temporal resolution compared to existing DREADDs, as SALB pharmacokinetics are relatively rapid; additionally, the KORD's effects are apparently robust. Finally, given the relative simplicity of multiplexing with bimodal control now easily achievable, the KORD will prove broadly useful for neuroscientists and other biologists.

EXPERIMENTAL PROCEDURES

Molecular Methods

Molecular Biology

Mutagenesis, radioligand binding, and functional assays were done exactly as described in Vardy et al. (2013).

Molecular Modeling

Molecular modeling of SALA and SALB in complex with the WT KOR was performed as previously described (Vardy et al., 2013). Modeling of SALA and SALB in complex with the KORD was achieved by in silico mutation of D138

to N in the respective WT KOR-ligand complexes, with subsequent energy minimization in SYBYL-X 2.1 (Tripos Force Field, Gasteiger-Hückel charges, distance-dependent dielectric constant = 4.0; non-bonded interaction cutoff = 8 Å; termination criterion = energy gradient < 0.05 kcal/(mol × Å) or 100,000 iterations).

Viral Production Methods

Virus Production

KORD (Table S2) in pcDNA 3.0 was cloned into a human synapsin (hSyn)-driven double-floxed pAAV vector derived from pAAV-HA-M4D-IRES-mCitrine. The pAAV-HA-KORD-IRES-mCitrine was then used for AAV9 production at the UNC Vector Core as described (Zhu et al., 2014).

Viral Infusion In Vivo

Mice were anesthetized with ketamine (120 mg/kg) and xylazine (18 mg/kg) (Sigma), and viral constructs (AAV-hSyn-DIO-HA-KOR DREADD, AAV-hSyn-mCherry, or AAV-hSyn-KOR DREADD + AAV-hSyn-hM3D) were stereotaxically injected bilaterally into the VTA/SN, or hypothalamic PVH or ARC (coordinates for VTA/SN: AP −3.1, ML ± 0.4, DV −5.0; coordinates for PVH: AP −0.65, ML ± 0.2, DV −4.7; coordinates for ARC: AP −1.5, ML ± 0.3, DV −5.7) using a 1.0-μl Hamilton Neuros 7001 KH syringe at a volume of 300 nL/side, at a rate of 100 nL/min for the VTA/SN; 25 nL/side, at a rate of 50 nL/min for the PVH; and 200 nL/side, at a rate of 50 nL/min for the ARC. After surgery, mice were returned to their cages for 2–3 weeks of recovery before behavioral or electrophysiological testing.

Slide Preparation and Immunohistochemistry

Animals were deeply anesthetized with an overdose of ketamine (400 mg/kg) and xylazine (40 mg/kg) and transcardially perfused with PBS (4°C, pH 7.4) followed by 4% PFA in 0.1 M phosphate buffer (4°C, pH 7.4). Brains were post-fixed overnight in 4% PFA, and subsequently cryopreserved in 30% sucrose in 0.1 M phosphate buffer. For confocal image collection, tissue sections containing the VTA/SN were cut into 40-μm sections using a sliding microtome (Leica SM2010 R) and stored in an ethylene glycol/sucrose-based cryoprotectant. For immunohistochemistry, tissue sections were washed in PBS (pH 7.4) three times, followed by 30 min of permeabilization in PBS with 0.3% Triton-X. Tissue sections were blocked in 5% normal donkey serum and PBS with 0.3% Triton-X for 1 hr, and incubated with 1:500 rabbit anti-HA (Cell Signaling, cat# 3724S, RRID: AB_1549585) and 1:500 mouse anti-mCherry (Abcam, cat# ab125096, RRID: AB_11133266) for 48 hr at 4°C. Subsequently, tissues were washed three times for 5 min in PBS with 0.3% Triton-X, and then incubated with Alexa 568 donkey anti-mouse and Alexa 647 donkey anti-rabbit secondary antibodies (1:250) for 24 hr at 4°C. Tissue sections were washed three times for 5 min in PBS with 0.3% Triton-X, followed by two 5-min washes with PBS (pH 7.4). A DAPI counterstain (300 nM) was applied in the first PBS wash step. Whole-tissue sections were imaged with an epifluorescent slide scanner at the UNC translational pathology lab. Confocal images of infected midbrain GABAergic neurons were taken using a Fluoview FV1000 with a 40× (NA 1.3) oil objective. To show co-expression of mCitrine and the HA-tagged KORD, the same staining protocol was observed, substituting an anti-GFP antibody recognizing mCitrine.

Quantification of Co-expression of M3-DREADD and KORDs

A total of three 40-μm sections containing the VTA/SN were taken from brains of three mice who had received multiplexed DREADD injections. In each section, a z stack was collected in the VTA using a 40× oil objective (300 × 300 μm field of view). Co-expression of DREADDs was calculated by counting total transduced cells (either KOR or M3 positive) and calculating the relative percentages expressing KOR alone, M3 alone, or KOR/M3. Cell counts were averaged within each animal, and data were analyzed using a Student's paired t test.

Behavioral Studies

SALB Evaluation in Control Mice

The analgesic-like effect of KOR-specific drugs was determined measuring the heat sensitivity of mice in a hot plate assay as previously described (White et al., 2015). The effect of such drugs on balance and motor coordination was assessed by the rotarod test (White et al., 2015). KOR activation has been strongly related to anhedonia (Todtenkopf et al., 2004); the anhedonic effects of KOR agonists were measured by ICSS in mice as previously described (Robinson et al., 2012). This operant behavioral method measures the value of electrical stimulation (brain stimulation reward or BSR) applied to the fibers of the medial forebrain bundle (MFB) at the level of the lateral hypothalamus and can be used to assess the reward-potentiating or reward-devaluing effects of drugs.

Animals

Adult (at least post-natal day 50) male and female Slc32a1$^{tm2(cre)Lowl}$/J (VGAT-*ires*-Cre; provided by Dr. Bradford Lowell, Harvard University) littermates were housed in a temperature- and humidity-controlled environment under a 12-hr light/dark cycle and had free access to food and water. All procedures were approved by the Institutional Animal Care and Use Committee (IACUC) of the University of North Carolina at Chapel Hill, the National Institute of Diabetes and Digestive and Kidney Diseases, or the National Institute on Drug Abuse, and were conducted according to the Guide for the Care and Use of Laboratory Animals (NIH publication no. 85-23, revised 2011).

Locomotor Studies

Locomotor activity was measured before and after treatment with vehicle (s.c. or i.p.), SALB (1.0–17.0 mg/kg s.c.), or CNO (i.p.) in 28 × 28 cm plexiglass chambers containing two sets of 16 infrared photobeams (MedAssociates). Data were collected with software (MED-PC v4.1; MedAssociates) that calculated the total distance traveled (cm) by measuring the position of the mouse every 60 ms. During test sessions mice were placed into the center of the chamber, and locomotion was measured for 60 min. During single-drug exposure sessions, mice were removed from the chambers, injected with drug (SALB, 1–10.0 mg/kg; CNO, 3.0 mg/kg; or vehicle), and returned to the chamber for 60 min of testing. During two-drug exposure sessions, mice were removed from the chambers after a 60-min baseline, injected with vehicle or 3.0 mg/kg CNO, returned to apparatus for 30 min, removed, injected with 17.0 mg/kg SALB or vehicle, and returned to the chambers for an additional 30 min of testing. Mice were habituated to vehicle injections for 2 days before testing. SALB was dissolved in DMSO and injected subcutaneously (s.c.) through a 27-gauge needle at a volume of 1 μL/g body weight using a Hamilton GASTIGHT 250-μL syringe. CNO was dissolved in 10% DMSO in saline and injected i.p. through a 27-gauge needle at a volume of 10 μL/g body weight. Drugs were administered in counterbalanced order using a within-subjects design. Drug effects were determined by the total distance traveled during the 60-min post-injection period or during each 30-min post-injection period. Dose effects were analyzed with repeated-measures ANOVA with post hoc Bonferroni t tests when $p < 0.05$. Individual drug determinations were compared to vehicle using paired t tests.

Mouse Handling for Feeding Studies

Mice (10- to 12-week-old males) were singly housed for at least 2.5 weeks following surgery and handled for 10 consecutive days before the assay to reduce stress response. Feeding studies were performed in home cages with ad libitum food access. Home cages were changed every day during food intake measurements to eliminate residual food crumbs in the bedding. CNO was administered at 1 mg per kg of body weight. Saline was delivered at the same volume as CNO to maintain consistency in the studies. SALB was administered at 10 mg/kg, dissolved in DMSO. DMSO was delivered at the same volume as SALB to maintain consistency. Mice with "missed" viral injections, incomplete "hits," or expression outside the area of interest were excluded from analysis after post hoc examination of mCherry and mCitrine expression.

Feeding Studies in SIM1-Cre Mice

During the light cycle, animals (*SIM1-cre*, n = 7; WT, n = 6) were injected with either DMSO (s.c.) or SALB (10 mg/kg; s.c.), and food intake was measured 1 hr after injection. A full trial consisted of assessing food intake from the study subjects after they received injections of DMSO on day 1 and SALB on day 2. Animals received a day "off" between trials before another trial was initiated. The food intake data from all days following DMSO/SALB injections were then averaged across four trials and combined for analysis.

Feeding Studies in AGRP-Ires-Cre Mice

Just before the onset of the dark cycle, animals (*AGRP-ires-cre*, n = 6; WT, n = 6) were injected with either DMSO (s.c.) or SalB (10 mg/kg; s.c.), and food intake was measured 1 hr after injection. A full trial consisted of assessing food intake from the study subjects after they received injections of DMSO

on day 1 and SalB on day 2. Animals received a day "off" between trials before another trial was initiated. The food intake data from all days following DMSO/SalB injections were then averaged across three trials and combined for analysis.

Feeding Studies with Multiplexed KOR and hM3Dq DREADD

During the light cycle, animals (*AGRP-ires-cre*, n = 10) were injected with saline (i.p.), CNO (1 mg/kg; i.p.), DMSO (s.c.), or CNO + SalB (10 mg/kg; s.c.), and food intake was monitored every 30 min for 3 hr after s.c. injection. A full trial consisted of assessing food intake from the study subjects after they received injections of saline on day 1, CNO on day 2, DMSO on day 3, and CNO + SalB on day 4. Animals received 3 days "off" between trials before another trial was initiated. The food intake data from all days were then averaged by condition across three trials and combined for analysis.

Whole-Cell Electrophysiology Experiments

The ability of KORD to generate a SALB-induced hyperpolarization was tested using whole-cell electrophysiology. Slices were checked for adequate expression of the target constructs via the mCitrine fluorescence, and those mice in which expression of constructs could not be identified were discarded. Using a potassium gluconate-based internal recording solution, whole-cell electrophysiological experiments were conducted in current-clamp at the RMP for each neuron. Following a 5-min stable baseline, 100 nM SALB was bath-applied for 10 min (VTA/SN^{VGAT}), 6 min (PVH^{SIM1}), or 7 min (ARC^{AgRP}) at a flow rate of 2 mL per minute. Average RMPs before and after the application of SALB were calculated, and results were presented as a shift from baseline RMP. Miniature IPSCs were recorded in the presence of tetrodotoxin (500 nM) and kynurenic acid (3 mM) to block AMPA and NMDA receptor-dependent postsynaptic currents. Neurons were held at −70 mV across all voltage-clamp recordings, and recording electrodes were filled with (in mM) 70 KCl, 65 potassium gluconate, 5 NaCl, 10 HEPES, 2 QX-314, 0.6 EGTA, 4 Na-ATP, 0.4 Na-GTP (pH 7.25), and 290–295 mOsm. After a 6-min stable baseline, SALB (100 nM) was bath-applied for 15 min, and recordings were continued during a 20-min washout period. mIPSCs were detected using ClampFit, and the frequency and amplitude of events were normalized to baseline.

SUPPLEMENTAL INFORMATION

Supplemental Information includes four figures and two tables and can be found with this article online at http://dx.doi.org/10.1016/j.neuron.2015.03.065.

AUTHOR CONTRIBUTIONS

E.V. and B.L.R. designed the strategy for creating KORD, which E.V. executed. E.V., J.E.R., and C.L. designed and executed the in vivo studies to validate KORD with supervision by B.L.R., C.J.M., and M.J.K. E.V., P.M.G., F.M.S., and X.-P.H. performed in vitro pharmacology with supervision by B.L.R.; R.H.J.O., H.Z., and D.J.U. performed stereotaxic viral injections with supervision by B.L.R.; R.H.J.O. performed immunofluorescent studies with supervision by J.S. and quantified images; K.L.W., H.Z., J.F.D., C.L., and J.E.R. performed behavioral studies with supervision by B.L.R., T.L.K., C.J.M., and M.J.K.; J.E.R. performed the initial yeast screen with supervision by B.L.R.; C.L., N.A.C., K.E.P., and C.M.M. performed electrophysiology studies with supervision by T.L.K. and M.J.K.; P.D.M. performed molecular modeling studies; E.V., J.E.R., C.L., M.J.K., and B.L.R. wrote the manuscript with assistance of all authors; and B.L.R. was responsible for the overall design and execution of these studies.

ACKNOWLEDGMENTS

This work was supported, in whole or in part, by the NIH BRAIN Initiative Grant UO1MH105892 (B.L.R. and T.L.K.) and by R01 DA017204 (B.L.R.), PO1DA035764 (B.L.R.), and the NIH-NIMH Psychoactive Drug Screening Program (B.L.R.); the Intramural Research Program of the NIH, The National Institute of Diabetes and Digestive and Kidney Diseases – NIDDK; DK075087, DK075089 (M.J.K.); and by R01AA019454, R00AA017668, NARSAD Young Investigator Award, and U01AA020911 (T.L.K.); and F31AA02228001 (N.A.C.), R01 AA018335 (C.J.M.), and F30 AA021312 (J.E.R.).

Received: November 3, 2014
Revised: March 2, 2015
Accepted: March 29, 2015
Published: April 30, 2015

REFERENCES

Agulhon, C., Boyt, K.M., Xie, A.X., Friocourt, F., Roth, B.L., and McCarthy, K.D. (2013). Modulation of the autonomic nervous system and behaviour by acute glial cell Gq protein-coupled receptor activation in vivo. J. Physiol. *591*, 5599–5609.

Alexander, G.M., Rogan, S.C., Abbas, A.I., Armbruster, B.N., Pei, Y., Allen, J.A., Nonneman, R.J., Hartmann, J., Moy, S.S., Nicolelis, M.A., et al. (2009). Remote control of neuronal activity in transgenic mice expressing evolved G protein-coupled receptors. Neuron *63*, 27–39.

Ansonoff, M.A., Zhang, J., Czyzyk, T., Rothman, R.B., Stewart, J., Xu, H., Zjwiony, J., Siebert, D.J., Yang, F., Roth, B.L., and Pintar, J.E. (2006). Antinociceptive and hypothermic effects of Salvinorin A are abolished in a novel strain of kappa-opioid receptor-1 knockout mice. J. Pharmacol. Exp. Ther. *318*, 641–648.

Aponte, Y., Atasoy, D., and Sternson, S.M. (2011). AGRP neurons are sufficient to orchestrate feeding behavior rapidly and without training. Nat. Neurosci. *14*, 351–355.

Armbruster, B.N., Li, X., Pausch, M.H., Herlitze, S., and Roth, B.L. (2007). Evolving the lock to fit the key to create a family of G protein-coupled receptors potently activated by an inert ligand. Proc. Natl. Acad. Sci. USA *104*, 5163–5168.

Atasoy, D., Betley, J.N., Su, H.H., and Sternson, S.M. (2012). Deconstruction of a neural circuit for hunger. Nature *488*, 172–177.

Balthasar, N., Dalgaard, L.T., Lee, C.E., Yu, J., Funahashi, H., Williams, T., Ferreira, M., Tang, V., McGovern, R.A., Kenny, C.D., et al. (2005). Divergence of melanocortin pathways in the control of food intake and energy expenditure. Cell *123*, 493–505.

Besnard, J., Ruda, G.F., Setola, V., Abecassis, K., Rodriguiz, R.M., Huang, X.P., Norval, S., Sassano, M.F., Shin, A.I., Webster, L.A., et al. (2012). Automated design of ligands to polypharmacological profiles. Nature *492*, 215–220.

Betley, J.N., Cao, Z.F., Ritola, K.D., and Sternson, S.M. (2013). Parallel, redundant circuit organization for homeostatic control of feeding behavior. Cell *155*, 1337–1350.

Boyden, E.S., Zhang, F., Bamberg, E., Nagel, G., and Deisseroth, K. (2005). Millisecond-timescale, genetically targeted optical control of neural activity. Nat. Neurosci. *8*, 1263–1268.

Conklin, B.R., Hsiao, E.C., Claeysen, S., Dumuis, A., Srinivasan, S., Forsayeth, J.R., Guettier, J.M., Chang, W.C., Pei, Y., McCarthy, K.D., et al. (2008). Engineering GPCR signaling pathways with RASSLs. Nat. Methods *5*, 673–678.

Deisseroth, K. (2011). Optogenetics. Nat. Methods *8*, 26–29.

Dell'Anno, M.T., Caiazzo, M., Leo, D., Dvoretskova, E., Medrihan, L., Colasante, G., Giannelli, S., Theka, I., Russo, G., Mus, L., et al. (2014). Remote control of induced dopaminergic neurons in parkinsonian rats. J. Clin. Invest. *124*, 3215–3229.

Dong, S., Rogan, S.C., and Roth, B.L. (2010). Directed molecular evolution of DREADDs: a generic approach to creating next-generation RASSLs. Nat. Protoc. *5*, 561–573.

Erlenbach, I., Kostenis, E., Schmidt, C., Hamdan, F.F., Pausch, M.H., and Wess, J. (2001). Functional expression of M(1), M(3) and M(5) muscarinic acetylcholine receptors in yeast. J. Neurochem. *77*, 1327–1337.

Fenalti, G., Giguere, P.M., Katritch, V., Huang, X.P., Thompson, A.A., Cherezov, V., Roth, B.L., and Stevens, R.C. (2014). Molecular control of δ-opioid receptor signalling. Nature *506*, 191–196.

Fenalti, G., Zatsepin, N.A., Betti, C., Giguere, P., Han, G.W., Ishchenko, A., Liu, W., Guillemyn, K., Zhang, H., James, D., et al. (2015). Structural basis for bifunctional peptide recognition at human δ-opioid receptor. Nat. Struct. Mol. Biol. *22*, 265–268.

Guettier, J.M., Gautam, D., Scarselli, M., Ruiz de Azua, I., Li, J.H., Rosemond, E., Ma, X., Gonzalez, F.J., Armbruster, B.N., Lu, H., et al. (2009). A chemical-genetic approach to study G protein regulation of beta cell function in vivo. Proc. Natl. Acad. Sci. USA *106*, 19197–19202.

Hooker, J.M., Munro, T.A., Béguin, C., Alexoff, D., Shea, C., Xu, Y., and Cohen, B.M. (2009). Salvinorin A and derivatives: protection from metabolism does not prolong short-term, whole-brain residence. Neuropharmacology *57*, 386–391.

Jain, S., Ruiz de Azua, I., Lu, H., White, M.F., Guettier, J.M., and Wess, J. (2013). Chronic activation of a designer G(q)-coupled receptor improves β cell function. J. Clin. Invest. *123*, 1750–1762.

Kane, B.E., Nieto, M.J., McCurdy, C.R., and Ferguson, D.M. (2006). A unique binding epitope for salvinorin A, a non-nitrogenous kappa opioid receptor agonist. FEBS J. *273*, 1966–1974.

Keiser, M.J., Setola, V., Irwin, J.J., Laggner, C., Abbas, A.I., Hufeisen, S.J., Jensen, N.H., Kuijer, M.B., Matos, R.C., Tran, T.B., et al. (2009). Predicting new molecular targets for known drugs. Nature *462*, 175–181.

Krashes, M.J., Koda, S., Ye, C., Rogan, S.C., Adams, A.C., Cusher, D.S., Maratos-Flier, E., Roth, B.L., and Lowell, B.B. (2011). Rapid, reversible activation of AgRP neurons drives feeding behavior in mice. J. Clin. Invest. *121*, 1424–1428.

Krashes, M.J., Shah, B.P., Madara, J.C., Olson, D.P., Strochlic, D.E., Garfield, A.S., Vong, L., Pei, H., Watabe-Uchida, M., Uchida, N., et al. (2014). An excitatory paraventricular nucleus to AgRP neuron circuit that drives hunger. Nature *507*, 238–242.

Larson, D.L., Jones, R.M., Hjorth, S.A., Schwartz, T.W., and Portoghese, P.S. (2000). Binding of norbinaltorphimine (norBNI) congeners to wild-type and mutant mu and kappa opioid receptors: molecular recognition loci for the pharmacophore and address components of kappa antagonists. J. Med. Chem. *43*, 1573–1576.

Li, J.H., Jain, S., McMillin, S.M., Cui, Y., Gautam, D., Sakamoto, W., Lu, H., Jou, W., McGuinness, O.P., Gavrilova, O., and Wess, J. (2013). A novel experimental strategy to assess the metabolic effects of selective activation of a G(q)-coupled receptor in hepatocytes in vivo. Endocrinology *154*, 3539–3551.

Magnus, C.J., Lee, P.H., Atasoy, D., Su, H.H., Looger, L.L., and Sternson, S.M. (2011). Chemical and genetic engineering of selective ion channel-ligand interactions. Science *333*, 1292–1296.

Mahler, S.V., Vazey, E.M., Beckley, J.T., Keistler, C.R., McGlinchey, E.M., Kaufling, J., Wilson, S.P., Deisseroth, K., Woodward, J.J., and Aston-Jones, G. (2014). Designer receptors show role for ventral pallidum input to ventral tegmental area in cocaine seeking. Nat. Neurosci. *17*, 577–585.

Nakajima, K., and Wess, J. (2012). Design and functional characterization of a novel, arrestin-biased designer G protein-coupled receptor. Mol. Pharmacol. *82*, 575–582.

Noble, B., Kallal, L.A., Pausch, M.H., and Benovic, J.L. (2003). Development of a yeast bioassay to characterize G protein-coupled receptor kinases. Identification of an NH2-terminal region essential for receptor phosphorylation. J. Biol. Chem. *278*, 47466–47476.

Portoghese, P.S. (1989). Bivalent ligands and the message-address concept in the design of selective opioid receptor antagonists. Trends Pharmacol. Sci. *10*, 230–235.

Robinson, J.E., Fish, E.W., Krouse, M.C., Thorsell, A., Heilig, M., and Malanga, C.J. (2012). Potentiation of brain stimulation reward by morphine: effects of neurokinin-1 receptor antagonism. Psychopharmacology (Berl.) *220*, 215–224.

Rogan, S.C., and Roth, B.L. (2011). Remote control of neuronal signaling. Pharmacol. Rev. *63*, 291–315.

Roth, B.L., Baner, K., Westkaemper, R., Siebert, D., Rice, K.C., Steinberg, S., Ernsberger, P., and Rothman, R.B. (2002). Salvinorin A: a potent naturally occurring nonnitrogenous kappa opioid selective agonist. Proc. Natl. Acad. Sci. USA *99*, 11934–11939.

Stachniak, T.J., Ghosh, A., and Sternson, S.M. (2014). Chemogenetic synaptic silencing of neural circuits localizes a hypothalamus→midbrain pathway for feeding behavior. Neuron *82*, 797–808.

Sternson, S.M., and Roth, B.L. (2014). Chemogenetic tools to interrogate brain functions. Annu. Rev. Neurosci. *37*, 387–407.

Strader, C.D., Gaffney, T., Sugg, E.E., Candelore, M.R., Keys, R., Patchett, A.A., and Dixon, R.A. (1991). Allele-specific activation of genetically engineered receptors. J. Biol. Chem. *266*, 5–8.

Todtenkopf, M.S., Marcus, J.F., Portoghese, P.S., and Carlezon, W.A., Jr. (2004). Effects of kappa-opioid receptor ligands on intracranial self-stimulation in rats. Psychopharmacology (Berl.) *172*, 463–470.

Tong, Q., Ye, C.P., Jones, J.E., Elmquist, J.K., and Lowell, B.B. (2008). Synaptic release of GABA by AgRP neurons is required for normal regulation of energy balance. Nat. Neurosci. *11*, 998–1000.

Urban, D.J., and Roth, B.L. (2015). DREADDs (designer receptors exclusively activated by designer drugs): chemogenetic tools with therapeutic utility. Annu. Rev. Pharmacol. Toxicol. *55*, 399–417.

van Zessen, R., Phillips, J.L., Budygin, E.A., and Stuber, G.D. (2012). Activation of VTA GABA neurons disrupts reward consumption. Neuron *73*, 1184–1194.

Vaqué, J.P., Dorsam, R.T., Feng, X., Iglesias-Bartolome, R., Forsthoefel, D.J., Chen, Q., Debant, A., Seeger, M.A., Ksander, B.R., Teramoto, H., and Gutkind, J.S. (2013). A genome-wide RNAi screen reveals a Trio-regulated Rho GTPase circuitry transducing mitogenic signals initiated by G protein-coupled receptors. Mol. Cell *49*, 94–108.

Vardy, E., Mosier, P.D., Frankowski, K.J., Wu, H., Katritch, V., Westkaemper, R.B., Aubé, J., Stevens, R.C., and Roth, B.L. (2013). Chemotype-selective modes of action of κ-opioid receptor agonists. J. Biol. Chem. *288*, 34470–34483.

White, K.L., Robinson, J.E., Zhu, H., DiBerto, J.F., Polepally, P.R., Zjawiony, J.K., Nichols, D.E., Malanga, C.J., and Roth, B.L. (2015). The G protein-biased κ-opioid receptor agonist RB-64 is analgesic with a unique spectrum of activities in vivo. J. Pharmacol. Exp. Ther. *352*, 98–109.

Wu, H., Wacker, D., Mileni, M., Katritch, V., Han, G.W., Vardy, E., Liu, W., Thompson, A.A., Huang, X.P., Carroll, F.I., et al. (2012). Structure of the human κ-opioid receptor in complex with JDTic. Nature *485*, 327–332.

Yagi, H., Tan, W., Dillenburg-Pilla, P., Armando, S., Amornphimoltham, P., Simaan, M., Weigert, R., Molinolo, A.A., Bouvier, M., and Gutkind, J.S. (2011). A synthetic biology approach reveals a CXCR4-G13-Rho signaling axis driving transendothelial migration of metastatic breast cancer cells. Sci. Signal. *4*, ra60.

Zhu, H., Pleil, K.E., Urban, D.J., Moy, S.S., Kash, T.L., and Roth, B.L. (2014). Chemogenetic inactivation of ventral hippocampal glutamatergic neurons disrupts consolidation of contextual fear memory. Neuropsychopharmacology *39*, 1880–1892.